Science Advances
AAAS

advances.sciencemag.org/cgi/content/full/7/1/eabb6104/DC1

Supplementary Materials for

Near-infrared oxidative phosphorylation inhibitor integrates acute myeloid leukemia–targeted imaging and therapy

Chi Zhang, Tao Liu, Peng Luo, Li Gao, Xingyun Liao, Le Ma, Zhongyong Jiang, Dengqun Liu, Zeyu Yang, Qingzhi Jiang, Yu Wang, Xu Tan, Shenglin Luo*, Yang Wang*, Chunmeng Shi*

*Corresponding author. Email: shicm@sina.com (C.S.); 200616wy@163.com (Y.W.); luosl@tmmu.edu.cn (S.L.)

Published 1 January 2021, *Sci. Adv.* **7**, eabb6104 (2021)
DOI: 10.1126/sciadv.abb6104

This PDF file includes:

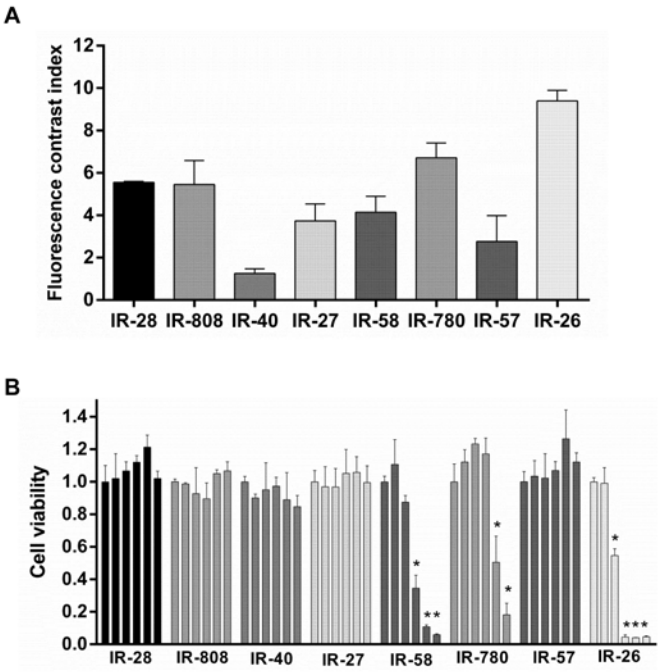

Fig. S1. Characterization of AML-targeted dyes. (**A**) Evaluating the accumulation and retention of different NIR dyes in AML cells when compared with PBMCs, and indicating IR-26 is the optimal choice for AML cells imaging. The fluorescence contrast index (CI) values were calculated according to the formula CI= F tumor/ F normal. F tumor is the fluorescence mean intensities of AML cells and F normal is the fluorescence mean intensities of PBMCs. The fluorescent intensity was calculated by flow cytometry (BD FACSVerseTM, BD Biosciences) with 633 nm excitation and 780 nm emission. (**B**) HL-60 cell lines were treated with a series of heptamethine cyanine dyes for 48 hours, and cell viability was measured (n=6). Error bars denote mean ±SD. *$P < 0.05$.

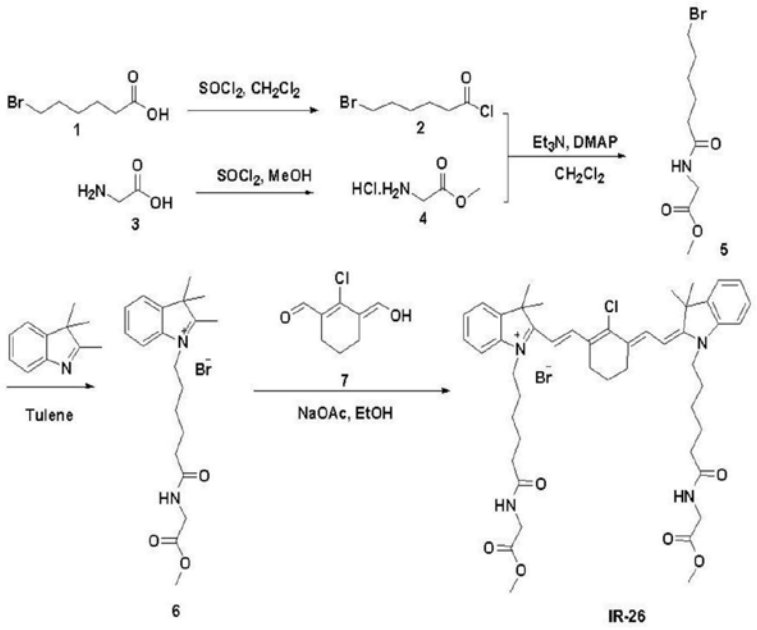

Fig. S2. Synthetic route and chemical structure of heptamethine cyanine dye, IR-26.

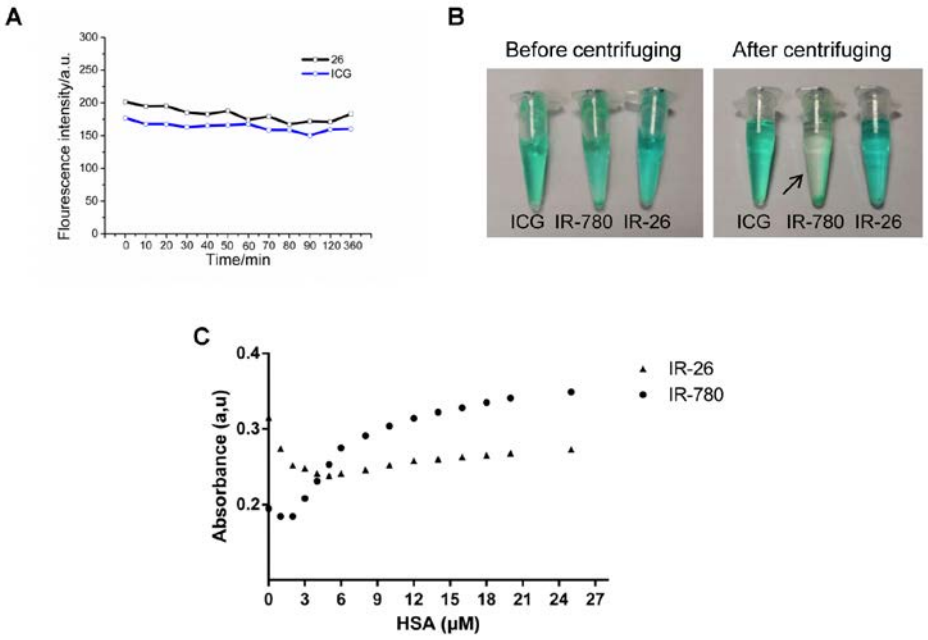

Fig. S3. The stability and dispersion of IR-26 in PBS and serum. (**A**) Fluorescence stability of IR-26 and indocyanine green (ICG) in 10% FBS at 37°C. (**B**) Images of ICG, IR-780, and IR-26 dissolved in the PBS solution before and after centrifuging (10000rpm, 10min). Photo credit: Yang Wang, Institute of Rocket Force Medicine, Third Military Medical University. (**C**) The absorption intensity of IR-26 and IR-780 at 800nm after added different concentrations of HAS.

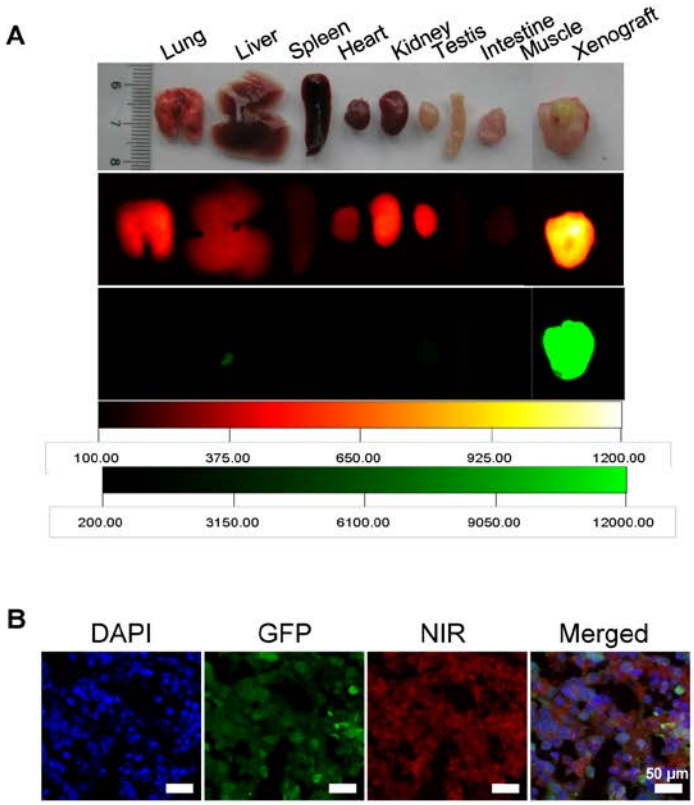

Fig. S4. Identifying the AML targeted property of IR-26 in mouse model. The GFP-labeled HL-60 cells were injected subcutaneously into the flank of nude mice to establish xenografts mouse model. (**A**) Mice were intravenously injected with IR-26 (0.2mg/kg), and the organs and xenografts were imaged using the Kodak In-Vivo Imaging System FX Pro. Photo credit: Chi Zhang, Institute of Rocket Force Medicine, Third Military Medical University. (**B**) Histopathologic analysis of xenografts from mice intravenously injected with IR-26 by confocal microscopy. Nuclei were stained with DAPI (blue).

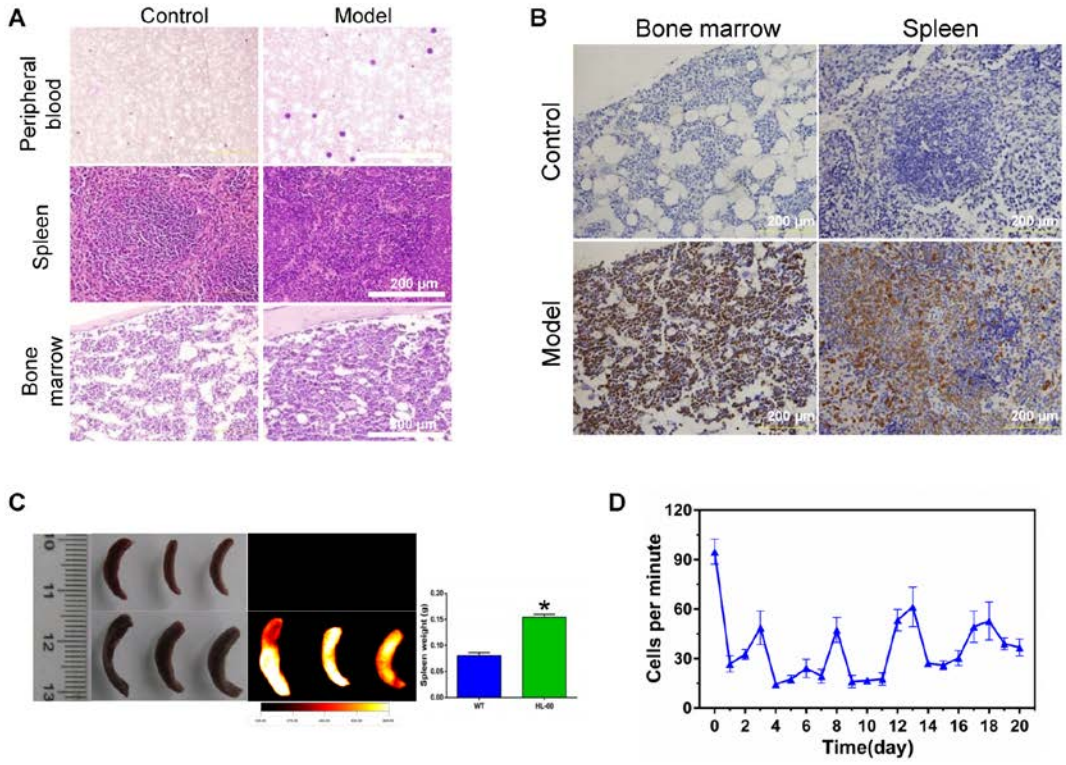

Fig. S5. Identification of the AML mouse model. GFP-labeled HL-60 cells were intravenous injected into the tail vein of sublethally irradiated C57 mice to establish AML mouse model. (**A**) Hematoxylin and eosin (H&E) staining of peripheral blood, spleen and bone marrow sections in control and transplanted mouse model. (**B**) Immunohistochemistry (IHC) analysis revealed GFP-labeled leukemia blasts were extensively infiltrated in the bone marrow and spleen of mouse model. (**C**) Spleens were weighted and imaged using a NIR imaging system after mouse injected with IR-26 (0.2mg/kg). Photo credit: Tao Liu, Institute of Rocket Force Medicine, Third Military Medical University. (**D**) The number of GFP-labeled HL-60 cells in the peripheral blood of mice model was monitored for 20 days using the in vivo flow cytometry (IVFC). Error bars denote mean ±SD. *P < 0.05.

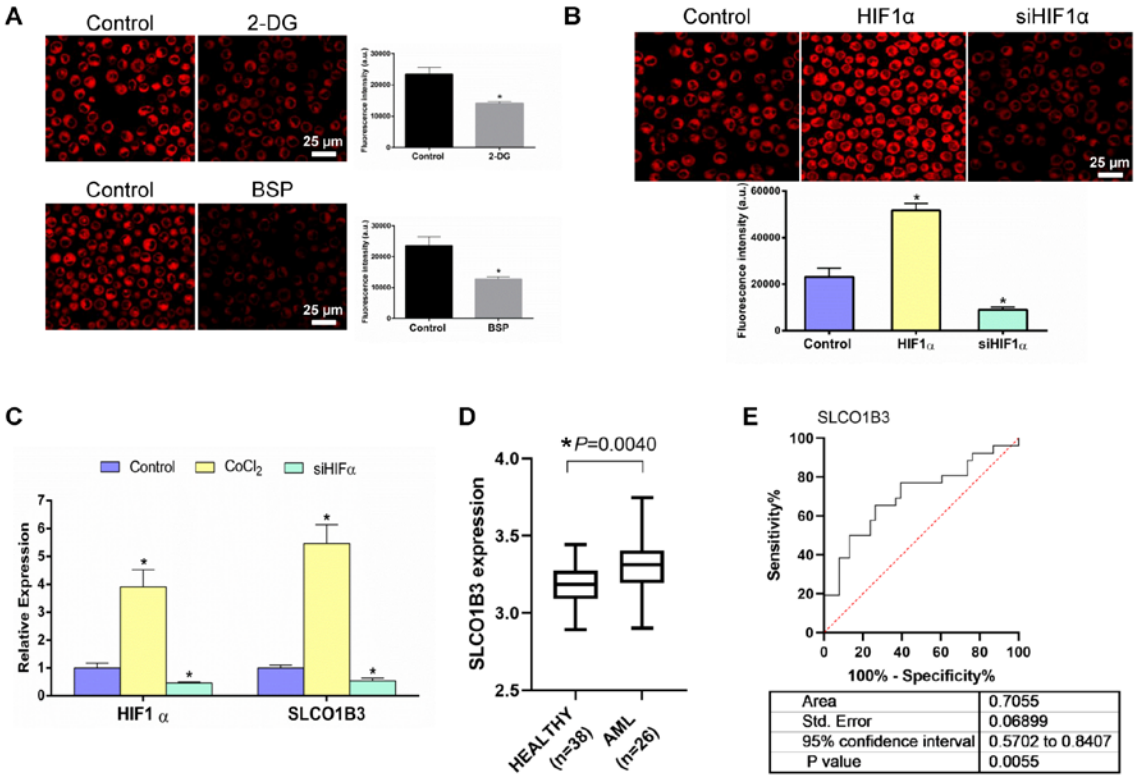

Fig. S6. Mechanic study of IR-26 targeting AML cells. (**A**) HL-60 cells were pretreated with glycolysis inhibitor 2-deoxy-D-glucose (2-DG, 150mM), or SLCO1B3 transporter sulfobromophthalein (BSP, 200μM), and then incubated with 10 μM IR-26 for 15 min prior to confocal microscopy observations. The fluorescence intensities of the samples were statistically analyzed (n=3). (**B**) HL-60 cells were pretreated with 0.1% dimethyl sulfoxide, $CoCl_2$ (200μM) or HIF-1α specific siRNA, and then incubated with 10 μM IR-26 prior to confocal microscopy observations. The fluorescence intensities of the samples were statistically analyzed (n=3). (**C**) The mRNA level of HIF-1α and SLCO1B3 were measured by real-time qPCR after cells were pretreated with dimethyl sulfoxide, $CoCl_2$ (200μM) or HIF-1α specific siRNA (n=3). (**D**) Analysis the expression of SLCO1B3 in clinic AML patients from the public data GSE9476. (**E**) Analysis the relationship of SLCO1B3 expression with AML patients from the public data GSE9476. Error bars denote mean ±SD. *P < 0.05.

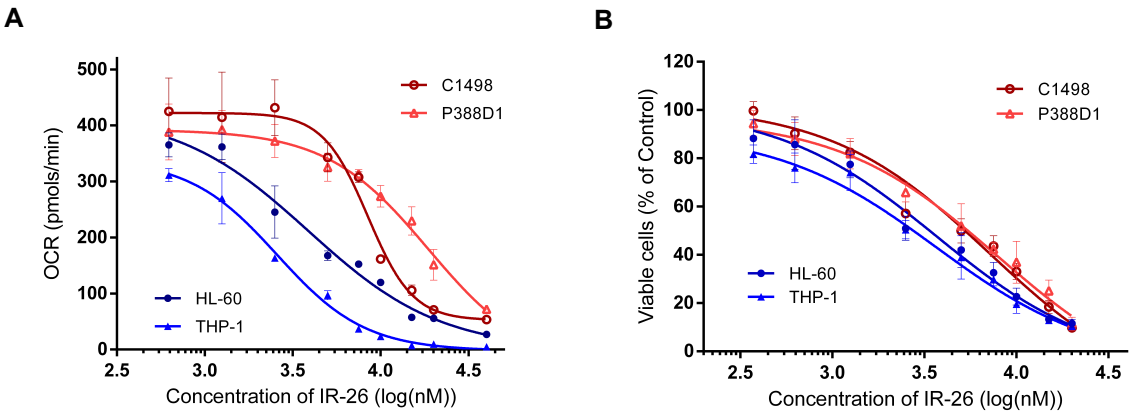

Fig. S7. Mouse and human cell lines (C1498, P388D1, HL-60 and THP-1) cells were treated with IR-26, and OCR (**A**) and the galactose viability (**B**) were measured after 1 or 48 h, respectively ($n = 3$).

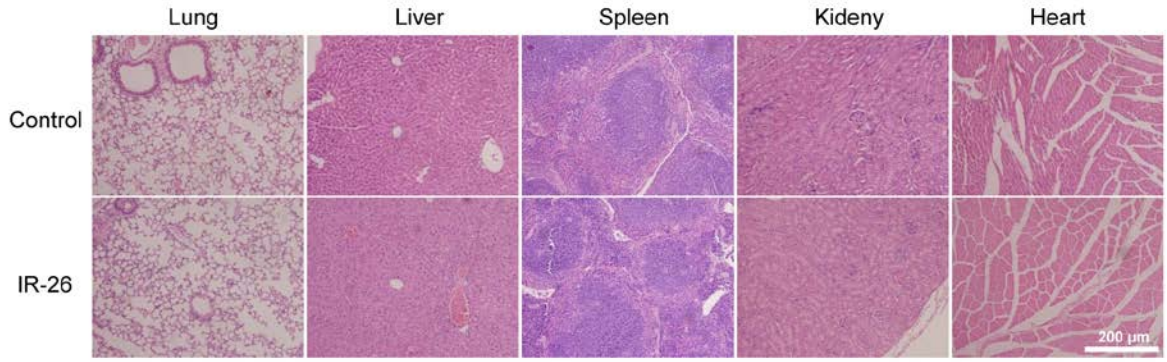

Fig. S8. Histopathologic analysis of vital organs in control and IR-26 treated mice; the figure indicated no obvious changes in the treatment mice.

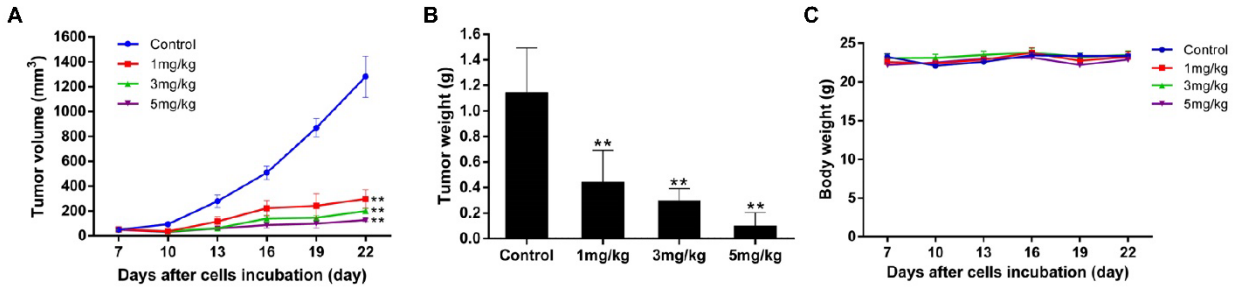

Fig. S9. IR-26 effectively inhibits tumor growth in nude mice bearing HL-60 subcutaneous xenografts among different concentrations. (**A**) Mice were treated with IR-26 (0, 1, 3, 5mg/kg every third day by i.p. injection), tumor volumes were measured and calculated as length× $(\text{width})^2/2$. (n =6, **P < 0.01 compared with control group). (**B**) The tumor weights were measured and compared (n =6, **P < 0.01 compared with control group). (**C**)The mice body weights were measured and compared (n =6).

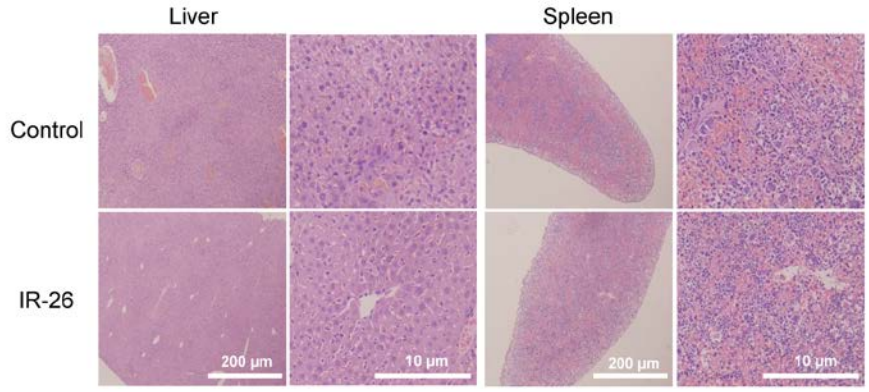

Fig. S10. Pathologic analysis of liver and spleen morphologic information in control and IR-26 treated mouse. GFP-labeled HL-60 cells were injected into the tail vein of NOD/SCID mice to establish orthotopic AML mouse model. Mice were treated with IR-26 (5mg/kg by intraperitoneal injection) or PBS as vehicle control.

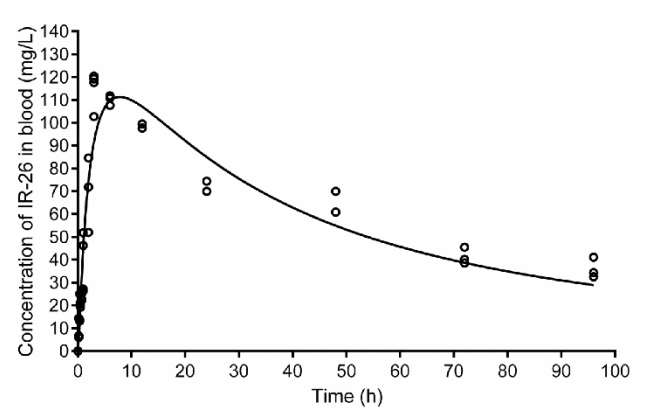

Fig. S11. In vivo blood curves of IR-26 in rat were determined based on IR-26 absorbance in the blood of normal mice after intraperitoneal injection (5mg/kg). The pharmacokinetic parameters were calculated (t1/2=56.43±6.38h, Cmax=115.23±6.73ug/L, Tmax=4±1.73h).